New magnetic dipole transition of the oxygen molecule: B 3 g X 3 g (0,0)

E. H. Roberts, K. L. Nixon, C. J. Dedman, S. T. Gibson, and B. R. Lewis

Citation: The Journal of Chemical Physics **116**, 5503 (2002); doi: 10.1063/1.1456506
View online: http://dx.doi.org/10.1063/1.1456506
View Table of Contents: http://scitation.aip.org/content/aip/journal/jcp/116/13?ver=pdfcov
Published by the AIP Publishing

New magnetic dipole transition of the oxygen molecule: $B'\,^3\Pi_g \leftarrow X\,^3\Sigma_g^-(0,0)$

E. H. Roberts, K. L. Nixon,[a] C. J. Dedman, S. T. Gibson, and B. R. Lewis
Research School of Physical Sciences and Engineering, The Australian National University, Canberra, ACT 0200, Australia

(Received 13 November 2001; accepted 10 January 2002)

Through the use of isotopically pure gas at a temperature of 77 K, a weak photoabsorption band of $^{16}O_2$ is found near 1856 Å, underlying the stronger Schumann–Runge (SR) band $B\,^3\Sigma_u^- \leftarrow X\,^3\Sigma_g^-(8,0)$. The location, structure, and intensity of this new band are consistent with expectation for the magnetic dipole transition $B'\,^3\Pi_g \leftarrow X\,^3\Sigma_g^-(0,0)$, where the designation B' is chosen to represent the $\mathrm{II}\,^3\Pi_g$ valence state. This electronic transition contributes to the ''excess absorption'' underlying the SR bands [B. R. Lewis, S. T. Gibson, and E. H. Roberts, J. Chem. Phys. **115**, 245 (2001)]. © *2002 American Institute of Physics.* [DOI: 10.1063/1.1456506]

I. INTRODUCTION

In the case of homonuclear diatomic molecules, $^3\Pi_g - {}^3\Sigma_g^{\pm}$ transitions are electric dipole forbidden by the $g \leftrightarrow u$ selection rule, but are allowed as magnetic dipole radiation, with expected intensities some five orders of magnitude weaker than for electric dipole allowed transitions.[1] While molecular oxygen has provided a number of examples of magnetic dipole transitions, e.g., $b\,^1\Sigma_g^+ - X\,^3\Sigma_g^-$ and $a\,^1\Delta_g - X\,^3\Sigma_g^-$, leading to the red[2] and infrared[3] atmospheric oxygen bands, respectively, there have been no previous reports of $^3\Pi_g - X\,^3\Sigma_g^-$ magnetic dipole transitions for this molecule.

In fact, experimental information on the $^3\Pi_g$ states of O_2 has arisen principally from electron energy loss (EEL) and (2+1) resonance-enhanced multiphoton-ionization (REMPI) spectroscopic studies, due to the different selection rules applying to these excitation mechanisms. These studies have been reviewed recently by Morrill *et al.*[4] Potential-energy curves for some of the lower-energy $^3\Pi_g$ states of O_2 are shown schematically in Fig. 1, in a diabatic (crossing) representation, together with adiabatic curves for the $X\,^3\Sigma_g^-$, $B\,^3\Sigma_u^-$, and $2\,^3\Sigma_g^-$ states. Discrete vibrational levels of the $3s\sigma_g\,C\,^3\Pi_g$ Rydberg state are well known.[4] However, only a little is known experimentally about the lowest two valence states, I, II, $^3\Pi_g$. First, the inner limb of the $\mathrm{II}\,^3\Pi_g$ state, in the region of its crossing with the *C* state, together with the value of the corresponding Rydberg-valence coupling (~620 cm^{-1}),[4] are defined by the experimental pattern of predissociation of the vibrational levels of the *C* state.[4–7] Second, the $\mathrm{I}\,^3\Pi_g \sim \mathrm{II}\,^3\Pi_g$ valence–valence coupling (~500 cm^{-1}),[4] can be deduced from the experimental photodissociation branching ratios for the lower *C*-state levels.[4,8] Finally, decompositions of the Schumann–Runge (SR) continua observed in EEL experiments have led to estimates of ~7.6 eV (~61 000 cm^{-1}) for the vertical $\mathrm{II}\,^3\Pi_g \leftarrow X\,^3\Sigma_g^-$ transition energy.[9,10]

An important conclusion following from the second of the above-mentioned observations is that the $^3\Pi_g$ valence states behave *diabatically* in the region of their crossing, due to the comparatively small value of the coupling involved.[8] Therefore, since the $\mathrm{II}\,^3\Pi_g$ state is bound, one would hope to be able to detect some of its lower (predissociated) vibrational levels. In a conventional single-photon absorption experiment, however, this task is made very difficult by strong competing absorption from the electric dipole allowed SR system $B\,^3\Sigma_u^- \leftarrow X\,^3\Sigma_g^-$, which, as can be seen from Fig. 1, overlaps the expected locations of the $\mathrm{II}\,^3\Pi_g \leftarrow X\,^3\Sigma_g^-$ bands.

In this work, operating so as to minimize spectral contamination by the SR system, we report the first observation of the magnetic dipole transition $\mathrm{II}\,^3\Pi_g \leftarrow X\,^3\Sigma_g^-(0,0)$. We rename the upper state of this transition $B'\,^3\Pi_g$ and use this nomenclature henceforth.[11]

II. EXPERIMENTAL METHOD

The choice of apparatus was governed principally by the need for a very high signal-to-noise ratio (S/N) in order to detect weak structure in the presence of significant competing absorption. Radiation from an H_2-continuum capillary discharge, operating at a dc current of 1.2 A, was passed through a 2.2 m scanning vacuum-ultraviolet monochromator,[12] providing a resolution of ~0.06 Å full width at half-maximum (FWHM). Some of the radiation exiting the monochromator was reflected from a slotted-Al beam splitter into a monitor photomultiplier, the remainder passing through a ~1 m long absorption cell, fitted with MgF_2 windows, into the detector photomultiplier. Both photomultipliers (EMR type 542F-09-17, CsTe photocathode) were operated in the pulse-counting mode, yielding typical signal count rates of ~10 kHz.

The absorption cell was operated at a temperature of 77 K by filling its surrounding annular jacket with liquid N_2. Low-temperature operation was essential in order to minimize spectral contamination by high-rotational lines of the SR $(v,0)$ system and eliminate the SR $(v,1)$ hot bands. The vacuum system surrounding the cell was filled with Ar at a pressure of ~0.2 Torr, as this was found to decrease the rate

[a]Present address: School of Chemistry, Physics, and Earth Sciences, The Flinders University of South Australia, Bedford Park, SA 5042, Australia.

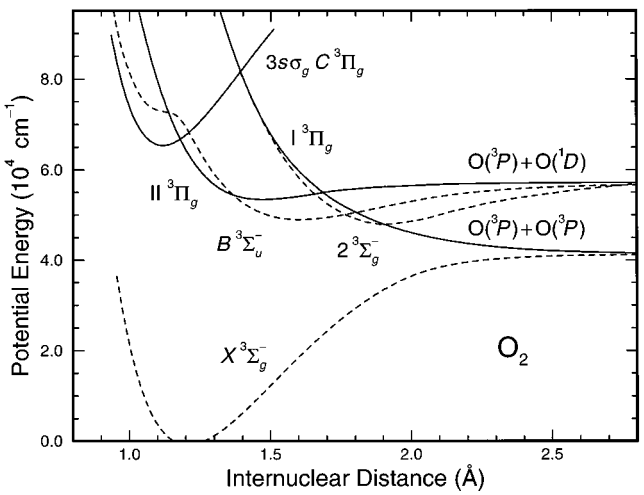

FIG. 1. Schematic potential-energy curves for the lowest-energy $^3\Pi_g$ states of O_2, shown in a diabatic (crossing) representation, (solid curves) together with adiabatic curves for the $X\,^3\Sigma_g^-$, $B\,^3\Sigma_u^-$, and $2\,^3\Sigma_g^-$ states (dashed curves). The $II\,^3\Pi_g(B'\,^3\Pi_g)$ valence state is the principal subject of this work.

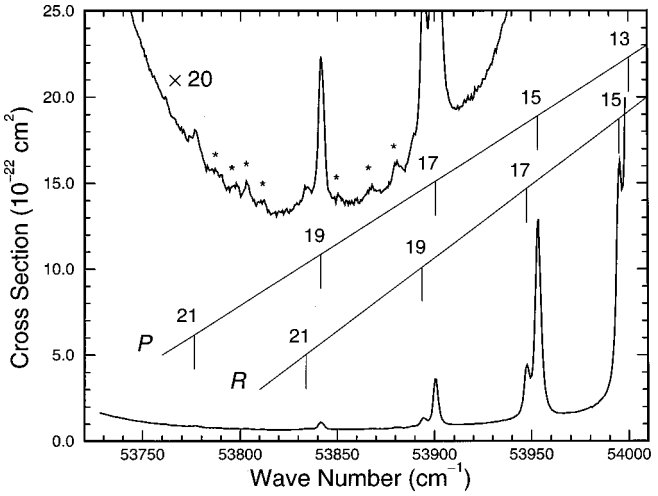

FIG. 2. Experimental photoabsorption cross section for pure $^{16}O_2$, measured at $T=77$ K and $P=100$ Torr, in the region of the cross-section minimum between the (7,0) and (8,0) Schumann–Runge band heads. $P(N'')$ and $R(N'')$ branch lines from the $B\leftarrow X(8,0)$ band are indicated. Weak features, marked with asterisks, and not belonging to the Schumann–Runge system, are apparent in the vertically expanded spectrum.

of degradation of cell-window transmittance caused by the inevitable deposition of condensible impurities during the experimental low-temperature runs. Wavelength scans were performed with the cell filled to a pressure of ~100 Torr of $^{16}O_2$ (ISOTEC, 99.993 atom%). The isotopically enriched sample was necessary in order to eliminate spectral contamination by the SR $(v,0)$ bands of $^{16}O\,^{18}O$, easily observable in the spectrum of normal O_2 which contains 0.41% $^{16}O\,^{18}O$.

Wavelength-dependent photoabsorption cross sections were determined from the cell transmittances using the Beer–Lambert law, with the effects of lamp-intensity fluctuations eliminated by normalizing the detector signal against the monitor signal. Because of the problem with cell-window transmittance degradation, for the most part, empty-cell transmittances were determined only at the start and end wavelengths of each scan. Thus, cross sections at intermediate wavelengths were subject to error since the window transmittances decreased nonlinearly with time during the scan. This problem is of minimal importance in the present work, however, where we are concerned primarily with the peak cross sections of relatively sharp spectral features, rather than the absolute value of the pressure-dependent background cross section. Data were accumulated for 30 s at each wavelength during individual scans, yielding a statistical uncertainty of ~0.3% in the cell transmittance. Since the weak spectral lines being sought in this work were only a factor of ~2 stronger than this level of uncertainty, it was necessary to average the experimental cross sections over ~20 scans in order to achieve a reasonable S/N. Absolute wavelength calibration was performed using the SR $(v,0)$ line positions of Yoshino *et al.*,[13] the embedded SR lines also serving as alignment points to minimize degradation of the effective wavelength resolution when averaging scans.

III. RESULTS AND DISCUSSION

The resulting experimental cross section in the region of the minimum between the $B\leftarrow X(7,0)$ and (8,0) band heads, uncorrected for pressure effects, is shown in Fig. 2. The principal $P(N'')$ and $R(N'')$ branches from the (8,0) band are visible in the spectrum for $N''\leqslant 21$. However, because of the low cell temperature of 77 K, no features attributable to satellite branches,[13] principal branches with $N''>21$,[13] or $v''>0$ hot bands[13] are discernible. Furthermore, the use of an isotopically pure $^{16}O_2$ sample has ensured that features arising from the $^{16}O\,^{18}O$ isotopomer[14] cannot be detected. Nevertheless, inspection of the vertically expanded spectrum in Fig. 2 reveals a number of previously unreported weak features, the strongest of which are indicated by asterisks, which are unrelated to the SR system and cannot be associated with any conceivable impurity.[15]

In order to assign the upper electronic state for the new ground-state transition responsible for these features, we consider which bound states of O_2 exist in the energy region of the observations, i.e., ~3300 cm^{-1} below the $O(^3P)+O(^1D)$ dissociation limit. The lowest Rydberg state of O_2 is the $3s\sigma_g\, C\,^3\Pi_g$ state,[16] shown in Fig. 1, the lowest vibrational level of which[4] lies ~12 000 cm^{-1} above the present energy region. Comprehensive *ab initio* calculations[17,18] of the valence states of O_2 show only two bound states in the relevant region; $1\,^3\Pi_g$ (the lower adiabatic state formed by the interacting $II\,^3\Pi_g$ and $I\,^3\Pi_g$ diabatic states of Fig. 1), and $2\,^3\Sigma_g^-$. Transitions from $X\,^3\Sigma_g^-$ to $^3\Pi_g$ and $^3\Sigma_g^-$ states are magnetic dipole and electric quadrupole allowed, respectively.[1] However, electric quadrupole transitions are much weaker than magnetic dipole transitions.[1] Furthermore, the $2\,^3\Sigma_g^-$ state lies at a large internuclear distance ($R_e=1.91$ Å,[18] see Fig. 1), implying negligible Franck–Condon overlap with the X state ($R_e=1.21$ Å[19]). Therefore, it appears that the only feasible candidate upper state for the weak transitions observed here is $B'\,^3\Pi_g$ (i.e., $1\,^3\Pi_g$ or $II\,^3\Pi_g$, in adiabatic or diabatic notation, respectively). This conclusion is supported qualitatively by an inspection of Fig. 2 which shows a band head near 53 810 cm^{-1}, with rotational struc-

ture degraded to the red, and additional subband structure lying ~100 cm^{-1} higher in energy. These characteristics are consistent only with a transition into a valence state having $\Lambda \geqslant 1$.[20] In the remainder of this work, we concentrate on testing the hypothesis that the weak features in Fig. 2 result from the $B'\,^3\Pi_g \leftarrow X\,^3\Sigma_g^-(0,0)$ magnetic dipole transition, through more detailed analyses of energy, rotational structure, and intensity.[21]

Spectroscopic constants for the $B'(v=0)$ state and the oscillator strength for the $B' \leftarrow X(0,0)$ transition were determined using a least-squares fitting procedure in which the fragmentary experimental cross section for the weak band was compared with a synthetic $^3\Pi \leftarrow {}^3\Sigma$ cross section. In this band model,[22] rotational energies and mixing coefficients for a $^3\Pi$ upper state with angular-momentum coupling intermediate between Hund's cases (a) and (b) were calculated using the effective Hamiltonian of Brown and Merer,[23] containing up to ten adjustable parameters, while intermediate energies, mixing coefficients, and Boltzmann factors for the $X\,^3\Sigma_g^-(v=0)$ state triplet components were calculated using the spectroscopic constants of Veseth and Lofthus.[24] Line centers for each of the 27 rotational branches characteristic of a $^3\Pi_g \leftarrow X\,^3\Sigma_g^-$ transition were then calculated using these energy levels.[25] Each rotational line was represented by a Voigt profile, with a Gaussian FWHM defined by the appropriate Doppler width (0.06 cm^{-1} FWHM at 77 K), and a Lorentzian (predissociation) FWHM for each subband which was a free parameter. Rotational line strengths, calculated using the methods described by Hougen,[26] were combined with the Boltzmann factors and a band oscillator strength which was a free parameter to determine the intensities of individual lines. The background cross section was fitted by a low-order polynomial in energy and instrumental effects were allowed for by convolution (in transmission) with a Gaussian of 1.7 cm^{-1} FWHM.

The results of the fitting procedure are illustrated in Fig. 3. The experimental cross section in Fig. 3 (solid circles) has been obtained from that of Fig. 2 by subtracting a smoothly varying background, in order to isolate the contributions arising from the newly observed transition. In addition, cross-section regions near the strong SR lines have been excised from the fit and are not displayed in Fig. 3.[27] The $^3\Pi_g \leftarrow X\,^3\Sigma_g^-$ band-model fit (solid curve in Fig. 3) provides a

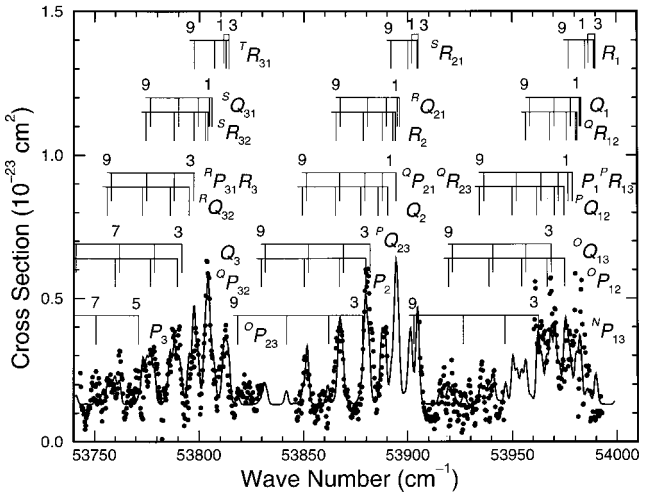

FIG. 3. Comparison between experimental cross section, following removal of contributions from the Schumann–Runge system, (solid circles) and the fitted $^3\Pi_g \leftarrow X\,^3\Sigma_g^-$ band-model cross section for $T=77$ K (solid curve). Gaps in the experimental spectrum coincide with strong $B \leftarrow X$ lines. The branch structure implied by the band-model fit is also indicated.

good description of the observed structure. However, it should be noted that the experimental S/N worsens considerably in the high-energy ($^3\Pi_0$) subband, where the SR photoabsorption cross section is increasing rapidly (see Fig. 2), leading to considerable fitting uncertainty in this region. Rotational-branch assignments for the fitted spectrum are indicated on Fig. 3, but no completely resolved lines are evident in the experimental spectrum. Wave numbers and assignments for the strongest of the observed blended features are listed in Table I.

Due to the limited experimental resolution and poor S/N, it was not possible to determine values significantly different from zero for many of the higher-order parameters in the Brown and Merer Hamiltonian.[23] Accordingly, λ, γ, and all of the centrifugal-distortion parameters were held fixed at zero during the final fitting procedure. In addition, although fitted values for the Λ-doubling parameters were not at all robust, the quality of the fit was definitely better for the two higher-energy subbands when Λ-doubling was nonzero. Finally, residual systematic discrepancies in the fit for the

TABLE I. Wave numbers and assignments for the strongest features observed in the $B'\,^3\Pi_g \leftarrow X\,^3\Sigma_g^-(0,0)$ band of O_2.

Subband	Wave number (cm^{-1})[a]	Assignment[b]
$^3\Pi_2$	53 811.6	$^TR_{31}(3), {}^TR_{31}(1), {}^TR_{31}(5)$
	53 803.8	$^SR_{32}(1), {}^SR_{32}(3), {}^SQ_{31}(3), {}^SQ_{31}(1), {}^TR_{31}(7)$
	53 797.8	$^RQ_{32}(3), {}^SR_{32}(5), {}^SQ_{31}(5), R_3(3)$
	53 788.4	$^RQ_{32}(5), {}^SQ_{31}(7), {}^SR_{32}(7), R_3(5), Q_3(3)$
$^3\Pi_1$	53 888.3[c]	$^RQ_{21}(5), {}^QR_{23}(3), {}^QP_{21}(3)$
	53 880.5	$^RQ_{21}(7), {}^PQ_{23}(3), {}^QR_{23}(5), {}^QP_{21}(5)$
	53 867.0	$^PQ_{23}(5), {}^RQ_{21}(9), {}^QR_{23}(7), {}^QP_{21}(7)$
	53 851.4	$^PQ_{23}(7), {}^QR_{23}(9), {}^QP_{21}(9)$
$^3\Pi_0$	53 969.4	$^PQ_{12}(5), {}^OP_{12}(3), {}^OQ_{13}(3), {}^QR_{12}(7), P_1(5), {}^PR_{13}(5), Q_1(7)$

[a]Wave number for center of broad line.
[b]Main contributing transitions, listed in order of decreasing strength.
[c]Shoulder.

TABLE II. Spectroscopic parameters for the $B'\,^3\Pi_g(v=0)$ state of O_2.

T^{ev} (cm^{-1})	53 889.0(3)[a]
$\nu_0(^3\Pi_1) \approx T^{ev}+2B$ (cm^{-1})	53 890.9(3)
B (cm^{-1})	0.960(4)
A (cm^{-1})	−86.0(3)
λ (cm^{-1})	0.0[b]
γ (cm^{-1})	0.0
$o+p+q$ (cm^{-1})	−0.9(4)
$p+2q$ (cm^{-1})	−0.2(5)
q (cm^{-1})	0.03(3)
f_{00}	$3.4(7)\times10^{-10}$
Γ_L (cm^{-1} FWHM)	0.2(4)

[a]3σ uncertainties of the fit are given in parentheses, in units of the last-quoted decimal place. Energy uncertainty does not include absolute calibration uncertainty.
[b]Parameters without uncertainties fixed during fit.

middle ($^3\Pi_1$) subband provide some evidence for a local perturbation in its rotational structure, although this conclusion is extremely tentative.

Final values for the fitted spectroscopic parameters are summarized in Table II. As shown below, the experimental values for the energy, rotational constant, and spin-orbit constant provide strong support for the $B'\,^3\Pi_g(v=0)$ assignment for the upper state of the transition. In Fig. 4, the multireference configuration-interaction plus Davidson correction (MRCI+Q) *ab initio* $1,2\,^3\Pi_g$ potential-energy curves of Partridge,[28] adjusted in energy to reproduce the experimental $O(^3P)+O(^1D)$ dissociation limit,[29] are shown (closed and open circles, respectively). If the avoided crossing is removed, then the diabatic I, II $^3\Pi_g$ potentials shown in Fig. 1 are obtained. The energy and rotational constant associated with the $v=0$ level of the II $^3\Pi_g$ MRCI+Q-derived potential are 53 810 and 0.959 cm^{-1}, respectively, in good agreement with the experimental values of Table II, $T^{ev}=53\,889\,cm^{-1}$ and $B=0.960\,cm^{-1}$, the energies differing by 79 cm^{-1}, i.e., only ~10% of the vibrational spacing. The experimental value for the $B'(v=0)$ diagonal spin-orbit constant, $A=-86\,cm^{-1}$, is consistent with the expectation of an inverted $^3\Pi_g$ state arising from the $\sigma_g\pi_g^3$ molecular-orbital configuration,[1] and is in quite good agreement with the *ab initio* calculation of Li *et al.*,[30] who find $A=-82\,cm^{-1}$ at $R=1.475$ Å, i.e., at the equilibrium internuclear distance of the MRCI+Q-derived II $^3\Pi_g$ state.

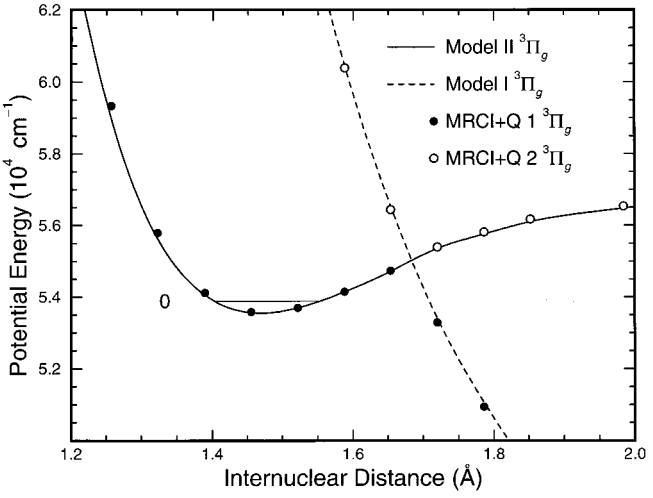

FIG. 4. Model diabatic $^3\Pi_g$ valence potential-energy curves (lines) compared with the MRCI+Q adiabatic curves of Ref. 28 (circles). The model potentials are referenced to an energy zero defined by the (nonexistent) $X\,^3\Sigma_g^-(v=0,J=N=0,F_2)$ level and the *ab initio* curves have been adjusted in energy to reproduce the experimental $O(^3P)+O(^1D)$ dissociation limit.

The transition moment for a $\Pi\leftarrow\Sigma(v',v'')$ transition may be estimated using the relation

$$M_{v'v''}(\text{a.u.}) = 406\sqrt{\frac{f_{v'v''}}{\nu_{v'v''}q_{v'v''}}}, \tag{1}$$

where $\nu_{v'v''}\,cm^{-1}$ is the transition energy, $f_{v'v''}$ is the oscillator strength, and $q_{v'v''}$ is the Franck–Condon factor. Using radial wave functions computed for the $v=0$ levels of a Rydberg–Klein–Rees potential for the X state[31] and the MRCI+Q-derived II $^3\Pi_g$ potential, we estimate a Franck–Condon factor $q_{00}\approx 9.0\times10^{-5}$ for the $B'\leftarrow X(0,0)$ transition. Substitution of this value into Eq. (1), together with the experimental oscillator strength of Table II, yields an estimate of $M_{00}=0.0034$ a.u. for the $B'\leftarrow X(0,0)$ transition moment. This order of magnitude is consistent with expectation for a magnetic dipole transition. For a $^3\Pi\leftarrow{}^3\Sigma$ transition, the magnetic dipole transition moment is given by[32]

$$|M(R)| = \frac{\alpha}{2}|\langle L^+(R)\rangle|, \tag{2}$$

where α is the fine-structure constant and $\langle L_+(R)\rangle$ is the expectation value of the angular-momentum raising operator between the $^3\Sigma$ and $^3\Pi$ states. Thus, using the estimated value of M_{00} in Eq. (2), a value of $|\langle L_{00}^+\rangle|=0.93$ a.u. can be estimated for the $B'\leftarrow X(0,0)$ transition. This is in reasonable agreement with the value 1.16 a.u. computed *ab initio* by Klotz *et al.*[33] at $R=1.21$ Å, but we note that our experiment samples $|\langle L^+(R)\rangle|$ at a considerably larger internuclear distance, $R\approx1.475$ Å.

In summary, the experimental band location, structure, and oscillator strength combine convincingly to support the assignment of the newly observed band as the magnetic dipole transition $B'\,^3\Pi_g\leftarrow X\,^3\Sigma_g^-(0,0)$. Unfortunately, the limited experimental resolution and poor S/N make it impossible to determine reliably the degree of predissociation of $B'(v=0)$. Nevertheless, it is likely that the predissociation line width Γ_L lies in the range 0.0–0.6 cm^{-1} FWHM (see Table II). Finally, we note that more definitive information on the B' state, particularly clarification of the possibilities of Λ-doubling and local perturbation, will require higher-resolution experiments employing different modes of excitation. Spin-orbit and rotational interactions between the $B'\,^3\Pi_g$ and $2\,^3\Sigma_g^-$ states provide the most likely explanation for any significant Λ-doubling and local perturbation. However, an accurate MRCI+Q-level potential-energy curve for the $2\,^3\Sigma_g^-$ state is required to test this proposition.

IV. COMPUTATIONAL MODEL

We have used the experimental results of Sec. III to construct a simple computational model for the B'-state spectroscopy and predissociation. The coupled-channel Schrödinger equation (CSE) technique,[34,35] which has been applied

extensively to O_2,[4,36–38] was used to compute photoabsorption cross sections for transitions between the X state and the valence–valence coupled I, II $^3\Pi_g$ states.

First, a diabatic two-channel CSE model of the upper states was constructed, consisting of the MRCI+Q-derived I, II $^3\Pi_g$ potential-energy curves coupled together by an R-independent electrostatic interaction $H^{el}=500\ cm^{-1}$.[4] Second, employing a least-squares fitting procedure in which the $B'(v=0)$ energies and rotational constants deduced from the CSE-computed $B'\leftarrow X$ cross sections were compared with the experimental values of Table II, the II $^3\Pi_g$ potential-energy curve was adjusted smoothly to optimize the agreement. The resulting diabatic model potentials (curves) are compared in Fig. 4 with the Partridge[28] MRCI+Q calculations. As expected from the discussion in Sec. III, minimal adjustments were required: the MRCI+Q-derived II $^3\Pi_g$ potential was shifted to smaller R by 3 mÅ,[39] while the well depth was decreased by 3%. These very small discrepancies between the experimental and MRCI+Q potentials are broadly consistent with those found for other electronic states of O_2.[40] As part of the least-squares fitting procedure, the magnetic dipole transition moment, assumed to be independent of R, was adjusted to produce agreement between the CSE-computed and experimental oscillator strengths. The final value, $M=0.0031(5)$ a.u., differs only marginally from the initial estimate of Sec. III and yields a final value of $|\langle L^+\rangle|=0.85(13)$ a.u. The CSE-computed $B'\leftarrow X(0,0)$ cross section yields a predissociation line width of 0.4 cm^{-1} FWHM, a value lying within the somewhat broad linewidth range determined experimentally. The origin of the B'-state predissociation is, of course, the valence–valence interaction between the II $^3\Pi_g$ and I $^3\Pi_g$ states.

Finally, we generalized the two-channel CSE model to a six-channel model in order to include the triplet structure of the upper states. Diabatic potential-energy curves for the II $^3\Pi_{g0}$ and II $^3\Pi_{g2}$ substates were obtained by shifting the optimized II $^3\Pi_{g1}$ curve in energy to reproduce the experimental diagonal spin-orbit constant of Table II. Those for the I $^3\Pi_{g0}$ and I $^3\Pi_{g2}$ substates were obtained by applying similar shifts to the MRCI+Q-derived I $^3\Pi_{g1}$ curve, since this valence state, arising from the $\sigma_u\pi_u^3$ molecular-orbital configuration, is also inverted. In addition to the valence–valence interaction H^{el} for each Ω substate, J-dependent **S**-uncoupling interactions between the substates within each $^3\Pi_g$ state[41] were also included in the model. The full $B'\leftarrow X(0,0)$ cross section computed for a temperature of 77 K using this six-channel CSE model[42] is shown in Fig. 5, both before and after convolution (in transmission) with a Gaussian instrumental function of 1.7 cm^{-1} FWHM. Overall agreement between the convolved CSE and experimental spectra is quite good, especially for the low-energy ($^3\Pi_2$) subband, confirming the utility of the model. However, systematic structural discrepancies arise in the $^3\Pi_1$ and, especially, $^3\Pi_0$ subbands, principally because the coupled-channel model of the upper states does not include the interactions with Σ states necessary to model Λ-doubling.

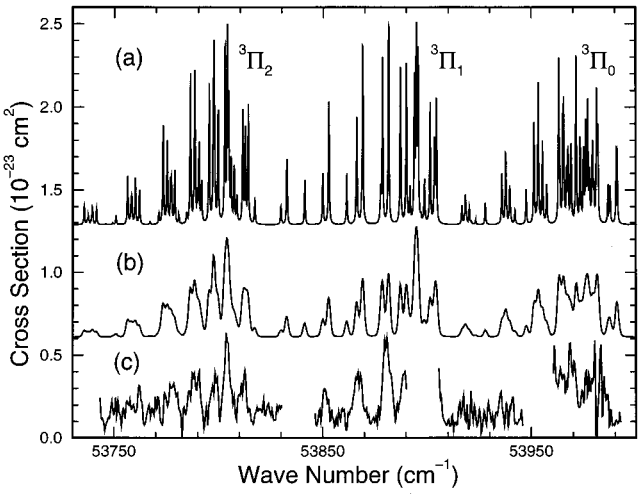

FIG. 5. Comparison between computed and experimental $T=77$ K cross sections for the $B'\,^3\Pi_g\leftarrow X\,^3\Sigma_g^-(0,0)$ magnetic dipole transition. (a) CSE-model computation. (b) CSE-model computation following instrument-function convolution. (c) Experimental cross section. For clarity, the computed cross sections have been shifted vertically.

V. SUMMARY AND CONCLUSIONS

The $B'\,^3\Pi_g\leftarrow X\,^3\Sigma_g^-$ magnetic dipole transition of the oxygen molecule has been observed for the first time, in the form of the weak $B'-X(0,0)$ band near 53 890 cm^{-1} (1856 Å) which underlies the electric dipole allowed Schumann–Runge band $B\,^3\Sigma_u^-\leftarrow X\,^3\Sigma_g^-(8,0)$. The experimental energy and rotational constant for the $B'(v=0)$ level are in good agreement with values deduced from the recent *ab initio* calculations of Partridge,[28] and the experimental magnetic dipole transition moment is in reasonable agreement with the *ab initio* calculations of Klotz *et al.*[33] The experimental results and theoretical model presented here are shown elsewhere[43] to provide support for the attribution of part of the ''excess absorption'' underlying the higher-vibrational Schumann–Runge bands to the $B'\,^3\Pi_g\leftarrow X\,^3\Sigma_g^-$ transition.[44]

ACKNOWLEDGMENTS

The authors would like to thank Dr. H. Partridge, for the supply of MRCI+Q *ab initio* potential-energy curves for the $^3\Pi_g$ states, and K. J. Lonsdale, for valuable technical assistance.

[1] G. Herzberg, *Molecular Spectra and Molecular Structure. I. Spectra of Diatomic Molecules* (van Nostrand, Princeton, 1950), pp. 277–279, 337.
[2] H. D. Babcock and L. Herzberg, Astrophys. J. **108**, 167 (1948).
[3] L. Herzberg and G. Herzberg, Astrophys. J. **105**, 353 (1947).
[4] J. S. Morrill, M. L. Ginter, B. R. Lewis, and S. T. Gibson, J. Chem. Phys. **111**, 173 (1999).
[5] R. S. Friedman and A. Dalgarno, J. Chem. Phys. **93**, 2370 (1990).
[6] R. S. Friedman, M. L. Du, and A. Dalgarno, J. Chem. Phys. **93**, 2375 (1990).
[7] A. Sur, L. Nguyen, and N. Nikoi, J. Chem. Phys. **96**, 6791 (1992).
[8] W. J. van der Zande, W. Koot, and J. Los, J. Chem. Phys. **91**, 4597 (1989).
[9] D. C. Cartwright, N. A. Fiamengo, W. Williams, and S. Trajmar, J. Phys. B **9**, L419 (1976).
[10] T. W. Shyn, C. J. Sweeney, A. Grafe, and W. E. Sharp, Phys. Rev. A **50**, 4794 (1994).

[11] We note that the nomenclature B' has been used in the past for the second mixed Rydberg-valence state of ${}^3\Sigma_u^-$ symmetry [D. H. Katayama, J. Chem. Phys. **89**, 5349 (1988)]. We prefer the accepted nomenclature $E\,{}^3\Sigma_u^-$ for this state [K. P. Huber and G. Herzberg, *Molecular Spectra and Molecular Structure: IV. Constants of Diatomic Molecules* (Van Nostrand Reinhold, New York, 1979, p. 494)], thus freeing the designation B' for the $\mathrm{II}\,{}^3\Pi_g$ state discussed here. Our choice of nomenclature is consistent with that accepted for the analogous state of the isovalent molecule S_2.
[12] B. R. Lewis, Appl. Opt. **22**, 1546 (1983).
[13] K. Yoshino, D. E. Freeman, and W. H. Parkinson, J. Phys. Chem. Ref. Data **13**, 207 (1984).
[14] A. S.-C. Cheung, K. Yoshino, D. E. Freeman, R. S. Friedman, A. Dalgarno, and W. H. Parkinson, J. Mol. Spectrosc. **134**, 362 (1989).
[15] Due to the low gas temperature, no condensible impurities can contribute to the spectrum.
[16] B. R. Lewis, S. T. Gibson, S. S. Banerjee, and H. Lefebvre-Brion, J. Chem. Phys. **113**, 2214 (2000).
[17] R. P. Saxon and B. Liu, J. Chem. Phys. **67**, 5432 (1977).
[18] H. H. Michels, Adv. Chem. Phys. **45**, 225 (1981).
[19] P. H. Krupenie, J. Phys. Chem. Ref. Data **1**, 423 (1972).
[20] In O_2, valence transitions are expected to be red-degraded, whereas unperturbed $3p$-Rydberg transitions will be blue-degraded, due to the relative magnitudes of the relevant rotational constants with respect to that of the X state.
[21] We anticipate the later conclusion that the $v=0$ level of the B' state is responsible for the observed transition.
[22] J. P. England, B. R. Lewis, and S. T. Gibson, *International Quantum Electronics Conference*, Anaheim, California, 1994 (unpublished).
[23] J. M. Brown and A. J. Merer, J. Mol. Spectrosc. **74**, 488 (1979).
[24] L. Veseth and A. Lofthus, Mol. Phys. **27**, 511 (1974).
[25] Band structures and intensity distributions for electric dipole-allowed ${}^3\Pi_u \leftarrow {}^3\Sigma_g^-$ and magnetic dipole-allowed ${}^3\Pi_g \leftarrow {}^3\Sigma_g^-$ transitions are similar, the different parity selection rules merely resulting in the swapping of the e/f parity labels in the upper state (see Ref. 1).
[26] J. T. Hougen, U.S. Natl. Bur. Stand. Monograph **115** (1970).
[27] A correction has been made for the contribution of the SR(8,0) $P(21)$ line weakly evident in Fig. 2, revealing further $B' \leftarrow X(0,0)$ structure in the ${}^3\Pi_2$ subband of Fig. 3 near 53 775 cm^{-1}.
[28] H. Partridge, personal communication; H. Partridge, C. W. Bauschlicher, Jr., S. R. Langhoff, and P. R. Taylor, J. Chem. Phys. **95**, 8292 (1991).
[29] The dissociation limit employed was a statistically weighted average over the atomic fine structure.
[30] Y. Li, I. D. Petsalakis, H.-P. Liebermann, G. Hirsch, and R. J. Buenker, J. Chem. Phys. **106**, 1123 (1997).
[31] P. C. Cosby, personal communication.
[32] R. S. Friedman and A. Dalgarno, J. Quant. Spectrosc. Radiat. Transf. **42**, 137 (1989).
[33] R. Klotz, C. M. Marian, S. D. Peyerimhoff, B. A. Hess, and R. J. Buenker, Chem. Phys. **89**, 223 (1984).
[34] E. F. van Dishoeck, M. C. van Hemert, A. C. Allison, and A. Dalgarno, J. Chem. Phys. **81**, 5709 (1984).
[35] L. Torop, D. G. McCoy, A. J. Blake, J. Wang, and T. Scholz, J. Quant. Spectrosc. Radiat. Transf. **38**, 9 (1987).
[36] B. R. Lewis, S. T. Gibson, J. S. Morrill, and M. L. Ginter, J. Chem. Phys. **111**, 186 (1999).
[37] J. P. England, B. R. Lewis, S. T. Gibson, and M. L. Ginter, J. Chem. Phys. **104**, 2765 (1996).
[38] B. R. Lewis, S. S. Banerjee, and S. T. Gibson, J. Chem. Phys. **102**, 6631 (1995).
[39] The shift in R differs slightly from the preliminary value -6 mÅ reported in Ref. 43, but the two values agree within the combined uncertainty estimates.
[40] B. Buijsse, W. J. van der Zande, A. T. J. B. Eppink, D. H. Parker, B. R. Lewis, and S. T. Gibson, J. Chem. Phys. **108**, 7229 (1998).
[41] J. W. C. Johns and D. W. Lepard, J. Mol. Spectrosc. **55**, 374 (1975).
[42] Details of the computation of full temperature-dependent cross sections using the CSE technique are discussed in detail in Ref. 38.
[43] B. R. Lewis, S. T. Gibson, and E. H. Roberts, J. Chem. Phys. **115**, 245 (2001).
[44] B. R. Lewis, L. Berzins, J. H. Carver, S. T. Gibson, and D. G. McCoy, J. Quant. Spectrosc. Radiat. Transf. **34**, 405 (1985).